ELSEVIER

Physics Reports 337 (2000) 171–192

PHYSICS REPORTS

www.elsevier.com/locate/physrep

Nematic liquid crystals under oscillatory shear flow

A.P. Krekhov[a,b,*], T. Börzsönyi[c,1], P. Tóth[a], Á. Buka[c], L. Kramer[a]

[a] *Physikalisches Institut, Universität Bayreuth, D-95440 Bayreuth, Germany*
[b] *Institute of Molecule and Crystal Physics, Russian Academy of Sciences, 450025 Ufa, Russia*
[c] *Research Institute for Solid State Physics and Optics, Hungarian Academy of Sciences, H-1525 Budapest, P.O.B. 49, Hungary*

Abstract

This contribution deals with three types of orientational phenomena generated by oscillatory flow in nematic liquid crystals: (1) Uniform orientational instabilities in the geometry where the director is initially oriented within the flow plane. The instability occurs under rectilinear Poiseuille flow and not under Couette flow. (2) The first instability under rectilinear Couette flow is a bifurcation to a stationary roll pattern with the roll axis perpendicular to the flow direction. The threshold amplitude has been measured for homeotropic alignment and calculated by linear stability analysis. (3) An interesting slow director precession and nonlinear waves which arise in homeotropically aligned nematics exposed to an elliptical shear flow in the bend Fréedericksz distorted state. The experimental data are compared with a theoretical analysis. The precession can also be generated by oscillatory compression.

PACS: 05.45. − a

Keywords: Instability of shear flows; Liquid crystals; Pattern formation

1. Introduction

In nematic liquid crystals (NLCs) the coupling between the preferred molecular orientation (director $\hat{\boldsymbol{n}}$) and the velocity field $\boldsymbol{v}$ leads to interesting flow phenomena. For a steady flow along the x-axis with a velocity field $v_x(z)$, $v_y = v_z = 0$ (rectilinear shear flow, typically of the Couette or Poiseuille type) the director will, in the absence of other torques, align in the flow plane (x–z plane) at the angle $\theta_{\mathrm{fl}} = \pm \arctan(\sqrt{\alpha_3/\alpha_2})$ (Leslie angle) with the x-axis if $\alpha_3/\alpha_2 > 0$ (the $\pm$ sign

* Corresponding author. Physikalisches Institut, Universität Bayreuth, D-95440 Bayreuth, Germany.
[1] Present address: Groupe de Physique des Solides, CNRS UMR 75-88, Universités Paris VI et VII, Tour 23, 2 place Jussieu, 75251 Paris Cedex 05, France.
E-mail address: alexei.krekhov@uni-bayreuth.de (A. Krekhov).

0370-1573/00/$ - see front matter
PII: S0370-1573(00)00061-2

corresponds to positive/negative shear rate $\partial v_x/\partial z$) [1,2]. Here α_3, α_2 are Leslie viscosity coefficients. In typical low-molecular-weight materials with rod-like molecules α_3/α_2 is small but positive (≈ 0.01), however, in some materials (in particular near a nematic–smectic transition) one has $\alpha_3/\alpha_2 < 0$ and instead of flow alignment there is a more complicated tumbling motion [3–5]. In the usual sample geometry the director is anchored at the boundaries and then one may have interesting instabilities and transitions that have been studied in the past, see e.g., [6–9].

When the velocity field oscillates periodically and symmetrically around zero (time average $\langle v_x(z,t)\rangle = 0$) the situation becomes richer. There are two quite different cases depending on whether the initial alignment of the director is perpendicular to the flow plane, i.e., in the y direction, or within the flow plane. The first case has been clarified in classical experiments by Pieranski and Guyon [10,11] and theoretical works of Dubois-Violette and Manneville (for an overview see [6]). For nematics with $\alpha_3 < 0$ one finds a transition to rolls oriented along the flow direction which transforms into a homogeneous distortion when a stabilising magnetic field is applied [11]. In the second case when the director is prealigned within the flow plane the dynamical behaviour under oscillatory flow can be quite complex. Some properties of this system which we have investigated in the last few years will be summarised here.

In Sections 2 and 3 we review briefly the experimental methods and the theoretical framework. Then, in Section 4, we present the equations for flow that is homogeneous in the plane of NLC layer and give solutions for the basic state under rectilinear oscillatory flow where the director oscillates around its equilibrium position induced by boundaries.

Next, we consider Fréedericksz-type instabilities where the time-averaged director reorients homogeneously in the plane of the layer (Section 5). For simple linear Couette flow no homogeneous instabilities are predicted to occur in contrast to the case of Poiseuille flow [12,13], even if the possibility of transitions out of the flow plane is included [13,14]. We consider only situations where the director lies initially in the shear plane. We have analysed the time-averaged (over the oscillation period) torques acting on the director in spatially homogeneous situations (no boundary conditions) [12,13]. For low-frequency Couette flow there are no torques whereas for Poiseuille flow there are torques directed away from the flow-alignment angles and, for $\theta > \theta_{\mathrm{fl}}$, away from the flow plane. Besides the weakly stable planar state $\hat{\boldsymbol{n}} = \hat{\boldsymbol{x}}$ (for flow-aligning materials) there exists a stationary attractor out of the flow plane. Numerical simulations confirm that for non-planar (homeotropic or oblique) boundary conditions above a critical flow amplitude an out-of-plane transition indeed occurs leading to the new stationary state [13,14]. Some recent experimental results on the orientational transition in homeotropically oriented NLCs under oscillatory Poiseuille flow will be presented.

In Couette flow with increasing flow amplitude one has found experimentally transitions to different roll states [15–17] (rolls axis perpendicular or parallel to the shear direction), which were not understood very well [16,18] (in the theory the elastic torque in the oscillatory part of the destabilising fluctuations has been neglected, which is a questionable approximation at low frequencies). In Section 6 we show our recent experimental and theoretical results. Comparison of the threshold amplitude of the roll instability between experiment and numerical linear stability analysis shows satisfactory agreement [19].

Elliptical shear flow (including circular as a special case), by applying oscillations $x(t) = A_x \sin\omega t$, $y(t) = A_y \sin(\omega t + \Phi)$ to one of the confining plates (or by applying the two rectilinear components to the two plates) is interesting also at small flow amplitudes below the

occurrence of any flow instability (it has been studied intensively in the past in view of roll instabilities [6,20–23]). In particular, in the presence of an electric field above the bend Fréedericksz transition, a slow precession of the in-plane director and associated phase waves are observed. The only previous study of the Fréedericksz distorted state in the presence of elliptic shear was carried out by Dreyfus and Pieranski [24]. In Section 7 our latest results on these phenomena are presented. Similar phenomena are observed under oscillatory compression at ultrasonic frequencies, where one has strong deviations from the linear velocity profile.

2. Experimental methods

A nematic layer of thickness d was confined between two glass plates. To obtain *rectilinear Couette flow* periodic motion of the upper plate [see Fig. 1(a)] was generated by loudspeakers, controlled by high-precision mechanical elements and it was detected by position-sensitive photodetectors. To obtain *elliptic Couette flow* the lower plate was also set into periodic motion (with appropriate phase shift). The thickness of the sample was adjustable in the range of $d = 10$–200 μm. Homeotropic boundary conditions were obtained on clean SnO_2-coated glass plates. For rectilinear shear the substance 5CB was used. The transmission of a parallel laser beam was detected between crossed polars for the analysis of the small amplitude (below the roll threshold) behaviour. The characteristics of the spatial patterns were studied by computer controlled digital image analysis of the sample between crossed polars.

In the case of elliptic shear substances with negative dielectric anisotropy (MBBA, MERCK-Phase5) have been investigated. A tilted director configuration was achieved by an applied voltage U across the cell.

The slow precession of the director generated by elliptic shear was studied by digital image analysis. The slow director precession can be revealed by an other type of excitation: *periodic compression* ($f = 1$–100 kHz) of the sample, which was realized by piezoelectric elements [25]. Other details of the set-up can be found in [19,26].

The set-up for *oscillatory Poiseuille flow* experiments consists of a nematic sample confined between two glass plates. The thickness d of the nematic layer was controlled by two spacers placed along the flow direction. The nematic liquid crystal MBBA was filled by capillary forces and for homeotropic alignment at the glass plates their surfaces were treated with the surfactant DMOAP. An oscillatory pressure difference between the two open sides of the cell was generated by two vertical cylinders accommodating pistons driven sinusoidally in opposing sense by an electromotor [see Fig. 1(b)]. Two cavities of adjustable volume were used for regulation of the amplitude of the applied pressure in the range from 1 to 20 kPa. This set-up allowed to study an oscillatory Poiseuille flow in the frequency range from 1 to 20 Hz. The transmitted light intensity between cross polars was measured by a photo detector in the microscope and/or by a CCD camera. Interfaces for the signal processing were either an A/D board or a frame grabber.

3. General formulation and dimensional analysis

The standard set of hydrodynamic equations governing the director orientation and the flow field for nematic liquid crystals (Leslie–Ericksen continuous formulation [7,27]) consists of the

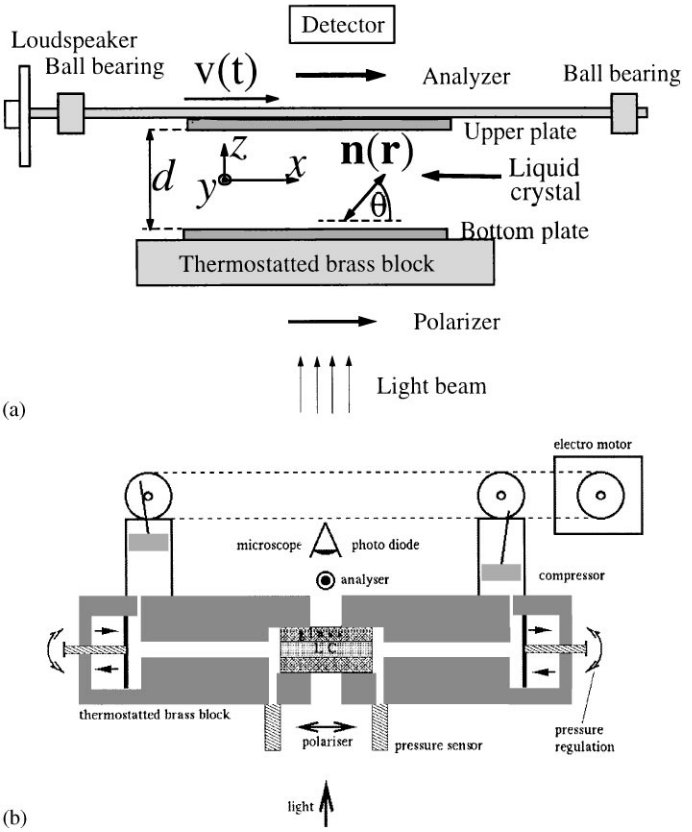

Fig. 1. Experimental setup for oscillatory Couette (a) and Poiseuille (b) flow.

director dynamic equation (balance of torques) involving the elasticities K_{11}, K_{22}, K_{33} and the rotational viscosities $\gamma_1 = \alpha_3 - \alpha_2$, $\gamma_2 = \alpha_6 - \alpha_5$, Navier–Stokes equation (momentum balance) involving the Leslie viscosities $\alpha_1, \ldots, \alpha_6$, incompressibility condition and director normalisation. These equations define two dynamic processes involved, which are described by two typical time scales:

$$\tau_{\mathrm{d}} = \frac{\gamma_1 d^2}{K_{33}}, \quad \tau_{\mathrm{v}} = \frac{\rho d^2}{\eta}\ , \tag{1}$$

where η is an appropriate shear viscosity of NLC which is of order of the rotational viscosity γ_1, representing relaxation times for the director (by bend elasticity) and the velocity field (by viscous damping). The ratio $\tau_{\mathrm{v}}/\tau_{\mathrm{d}}$ is typically very small ($\sim 10^{-6}$) thus the relaxation of the velocity fluctuations is much faster than the orientational relaxation. Then one can eliminate adiabatically the velocity field, i.e., discard the inertia of the mass flow. For a nematic layer of the thickness d under an oscillatory flow with frequency $f = \omega/(2\pi)$ one has natural dimensionless variables

$$\tilde{\boldsymbol{r}} = \boldsymbol{r}/d, \quad \tilde{t} = t\omega, \quad \tilde{\boldsymbol{v}} = \boldsymbol{v}/(\mathrm{d}\omega)\ , \tag{2}$$

and the nematohydrodynamic equations contain the dimensionless quantities

$$\varepsilon = (\tau_d \omega)^{-1}, \quad \delta = \tau_v \omega = \frac{d^2}{l^2} , \tag{3}$$

where $l = \sqrt{\eta/(\rho\omega)}$ is the viscous penetration depth. All additional dimensionless quantities appearing in the basic equations involve ratios of the elasticities and viscosities which are mostly of order 1. The only exception of some relevance in the following is $\lambda = \alpha_3/\alpha_2$. Oscillatory motion of the confining plates (Couette flow) or application of oscillatory pressure gradient (Poiseuille flow) introduce the dimensionless control parameter $a = A/d$ where A is a flow displacement amplitude. One can introduce for our problem the Ericksen number which is a measure of the effect of the flow on the director orientation (viscous stress/elastic stress)

$$Er = a/\varepsilon . \tag{4}$$

Since the ratio τ_d/τ_v is also a material constant, the response of a given NLC depends on d, ω and A only through ε (or δ) and a. As a result the critical flow amplitude for a particular orientational instability is a universal function depending only on the product ωd^2 (or $\tau_d \omega$).

4. Homogeneous flow

We first look for solutions of the nematohydrodynamic equations where the director $\hat{\boldsymbol{n}}$ and the velocity $\boldsymbol{v}$ are functions only of the transverse coordinate z and time t

$$\hat{\boldsymbol{n}} = \{n_x(z,t), n_y(z,t), n_z(z,t)\} ,$$
$$\boldsymbol{v} = \{v_x(z,t), v_y(z,t), 0\} . \tag{5}$$

Clearly the incompressibility condition $\nabla \cdot \boldsymbol{v} = 0$ is satisfied. Setting

$$N = n_x + \mathrm{i}n_y, \quad V = v_x + \mathrm{i}v_y , \tag{6}$$

one can rewrite the nematohydrodynamic equations [7,27] (consisting of the director torque balance and Navier–Stokes equation) in complex notation

$$\begin{aligned} N_{,t} = {} & \frac{n_z}{(1-\lambda)}\left(V_{,z} - \frac{1+\lambda}{2} N(N\bar{V}_{,z} + \bar{N}V_{,z}) \right) \\ & - \varepsilon\{k_1 n_z n_{z,zz} N - [N_{,zz} - N(N\bar{N}_{,zz} + \bar{N}N_{,zz})/2] \\ & + (1-k_2)[N(B^2 + iB_{,z})/2 + iN_{,z}B] - \pi^2 e^2 n_z^2 N + \pi^2 h^2 [N(\hat{\boldsymbol{m}}\cdot\hat{\boldsymbol{n}})^2 - (\hat{\boldsymbol{m}}\cdot\hat{\boldsymbol{n}})M]\} , \end{aligned} \tag{7}$$

$$\begin{aligned} \delta V_{,t} = {} & -p_{0,\eta} + \partial_z\{\alpha_2 n_z N_{,t} + \alpha_3 n_{z,t} N + \left[\frac{1}{2}(-\alpha_2 + \alpha_4 + \alpha_5) - \frac{1}{2}(-\alpha_2 + \alpha_5)|N|^2\right] V_{,z} \\ & + \frac{1}{2}\left[\frac{1}{2}(\alpha_3 + \alpha_6) + \alpha_1(1-|N|^2)\right] N(N\bar{V}_{,z} + \bar{N}V_{,z})\} \end{aligned} \tag{8}$$

with $n_z \equiv \sqrt{1-|N|^2}$, $B \equiv \mathrm{i}(N\bar{N}_{,z} - \bar{N}N_{,z})$, $f_{,i}$ denote derivatives, $\partial_\eta = \partial_x + \mathrm{i}\partial_y$ and

$$k_i = K_{ii}/K_{33}, \quad \tilde{\alpha}_i = \alpha_i/\gamma_1, \quad \gamma_1 = \alpha_3 - \alpha_2 \ ,$$

$$e = E/E_\mathrm{F}, \quad E_\mathrm{F} = \frac{\pi}{d}\sqrt{\frac{K_{33}}{\varepsilon_0|\varepsilon_a|}}, \quad h = H/H_\mathrm{F}, \quad H_\mathrm{F} = \frac{\pi}{d}\sqrt{\frac{K_{33}}{\mu_0\chi_a}} \ , \tag{9}$$

where the tildes have been omitted and E_F, H_F are the electric and magnetic bend Fréedericksz transition fields, respectively. In Eq. (7) we include the effect of electric field $\boldsymbol{E} = (0,0,E)$ and a magnetic field $\boldsymbol{H} = H(m_x, m_y, m_z)$ with $\hat{\boldsymbol{m}}^2 = 1$, $M = m_x + \mathrm{i}m_y$ which we will need later on.

Boundary conditions for the velocity for the rectilinear Couette flow are

$$p_0 = 0, \quad V(z = +\tfrac{1}{2}) = a\cos t, \quad V(z = -\tfrac{1}{2}) = 0 \ , \tag{10}$$

where $a = A/d$ with A the displacement amplitude. For the rectilinear Poiseuille flow one has

$$p_{0,\eta} = a_p \cos t, \quad V(z = \pm\tfrac{1}{2}) = 0 \tag{11}$$

and $a_p = (\Delta P/\Delta x)d/(\gamma_1\omega)$ ($\Delta P/\Delta x$ is the applied pressure gradient in physical units). This is to be supplemented by the boundary conditions for the director.

In the basic state solution for rectilinear flow $\hat{\boldsymbol{n}}$ and $\boldsymbol{v}$ remain confined to the flow plane

$$\hat{\boldsymbol{n}} = \{\cos\theta_0(z,t), 0, \sin\theta_0(z,t)\}, \quad \boldsymbol{v} = \{v_{0x}(z,t), 0, 0\} \ . \tag{12}$$

For the director we consider two cases, the limit of strong homeotropic anchoring

$$\theta_0(z = \pm\tfrac{1}{2}) = \pi/2 \tag{13}$$

and the weak-anchoring limit, which corresponds to torque-free boundary conditions

$$\theta_{0,z}(z = \pm\tfrac{1}{2}) = 0 \ . \tag{14}$$

The solution $\theta_0(z,t)$, $v_{0x}(z,t)$ of Eqs. (7) and (8) exists for all flow amplitudes, but may lose stability at some critical amplitude (see Section 6). In the low-frequency range to be considered here one has $\delta \ll 1$ (with $\rho \approx 10^3$ kg/m^3, $\eta \approx 10^{-1}$ N s/m^2 and $d \approx 10^{-4}$ m one has $\delta < 0.1$ for frequencies $f < 150$ Hz) and it is reasonable to neglect the inertia of the mass flow [left-hand side of Eq. (8)] (this was checked in simulations). Then analytic progress is possible in two limiting cases:

(i) Omitting the elastic coupling terms on the right-hand side of Eq. (7) one easily finds for Couette flow

$$\theta_0(t) = \frac{\pi}{2} - \arctan\left\{\frac{1}{\sqrt{\lambda}}\tanh\left[\frac{\sqrt{\lambda}}{1-\lambda}\,a\sin(t)\right]\right\} , \tag{15}$$

$$v_{0x}(z,t) = a(z + \tfrac{1}{2})\cos(t) \ , \tag{16}$$

so that the director is independent of z [28,14]. For Poiseuille flow one gets after integration of Eq. (8) and elimination of v_{0x} from Eq. (7)

$$\int \frac{Q(\theta_0) - K^2(\theta_0)}{K(\theta_0)}\,\mathrm{d}\theta_0 = a_p z \sin(t) \ ,$$

$$K(\theta) = \frac{\lambda\cos^2\theta - \sin^2\theta}{1-\lambda} \ ,$$

$$2Q(\theta) = \alpha_4 + (\alpha_5 - \alpha_2)\sin^2\theta + (\alpha_3 + \alpha_6 + 2\alpha_1\sin^2\theta)\cos^2\theta \ . \tag{17}$$

The integral on the left-hand side of Eq. (17) can be calculated analytically giving the expression for $\theta_0(z,t)$ in an implicit form [29].

For torque-free boundary conditions (14), Eqs. (15), (16) and (17) are exact solutions of (7) and (8) with the inertia term dropped. For strong anchoring (13) the omitted terms control the behaviour near the boundaries, where one has boundary layers of thickness $\sqrt{\varepsilon}$ (in physical units $\sqrt{K_{33}/\gamma_1\omega}$), which corresponds to the orientational diffusion length that is neglected here. So then one needs the condition $\varepsilon \ll 1$, i.e., $\omega \gg 1/\tau_d$ (for typical material parameters $K_{33} \approx 10^{-11}$ N, $\gamma_1 \approx 10^{-1}$ N s/m^2 and $d \approx 10^{-4}$ m one has $1/\tau_d = 0.01$ s^{-1}).

(ii) For the case of small distortions of the director away from the homeotropic orientation we write $\theta_0 = \pi/2 + \tilde{\theta}_0$, $v_{0x} = \tilde{v}_{0x}$ with $|\tilde{\theta}_0| \ll 1$, $|\tilde{v}_{0x}| \ll 1$ and linearise Eqs. (7), (8) with respect to $\tilde{\theta}_0$, $\tilde{v}_{0x}$. Then the solution in the form

$$\tilde{\theta}_0(z,t) = \theta_{01}(z)\cos t + \theta_{02}(z)\sin t\ ,$$
$$\tilde{v}_{0x}(z,t) = v_{01}(z)\cos t + v_{02}(z)\sin t \tag{18}$$

can be easily found [30,29]. The director oscillates periodically around the homeotropic orientation $\theta_0 = \pi/2$ and there is a frequency-dependent phase shift of these oscillations relative to the flow oscillations.

The homogeneous solutions [cases (i) and (ii)] have been investigated experimentally for rectilinear oscillatory Couette flow and a good quantitative agreement was found when compared with theory [19].

5. Homogeneous instabilities

5.1. Stability of the flow-alignment solution

Let us look at the special case when the director is oriented within the flow plane (x–z plane) at the flow-alignment angle θ_{fl} [Leslie angle, $\theta_{fl} = \arctan(\sqrt{\lambda})$] at $z = \pm 1/2$. Then the basic state corresponds to the simple flow-alignment solution

$$\hat{\boldsymbol{n}} = \{\cos\theta_{fl}, 0, \sin\theta_{fl}\}, \quad \upsilon = \{v_{0x}(z,t), 0, 0\} \tag{19}$$

of Eqs. (7) and (8). In case of steady flow this solution is stable for any flow amplitude [2,7]. We performed the linear stability analysis of the solution (19) for rectilinear oscillatory flow and found that for any flow with $v_{0x,zz} \neq 0$ the flow-alignment solution becomes unstable at some critical flow amplitude [14]. For oscillatory Poiseuille flow the (dimensionless) critical flow amplitude [14]

$$a_c = \frac{\pi\sqrt{2}}{8K'(\theta_{fl})} \tag{20}$$

independent of frequency (for $\delta \ll 1$). The corresponding result for oscillatory Couette flow

$$a_c = j_{1/4}2\sqrt{2}\frac{Q(\theta_{fl})\gamma_1}{\rho\omega d^2 K'(\theta_{fl})}\ , \tag{21}$$

where $j_{1/4} = 2.78088$ is the minimal positive root of the Bessel function $J_{1/4}(j_{1/4}) = 0$ [31].

From direct numerical simulations of Eqs. (7) and (8) we find that the flow-alignment solution becomes unstable as for oscillatory Poiseuille flow as for Couette flow at some critical amplitude. The critical amplitude for Poiseuille flow decreases slightly with increasing frequency ($2.5 \geq a_c \geq 2.3$ for 5 Hz $\leq f \leq 100$ Hz) which is near to the value $a_c = 2.78$ obtained from the linear stability analysis in case of prescribed velocity field. The agreement with Eq. (21) for Couette flow is also very good [31].

5.2. *Time-averaged approach*: *out-of-plane transition*

Let us now analyse the nonlinear director evolution. Introducing

$$\hat{\boldsymbol{n}} = \{\cos\theta(z,t)\cos\phi(z,t), \quad \sin\phi(z,t), \quad \sin\theta(z,t)\cos\phi(z,t)\}\ ,$$
$$\boldsymbol{v} = \{v_x(z,t), v_y(z,t), 0\}, \tag{22}$$

where θ is the angle with respect to the x-axis within the flow plane and ϕ is the out-of-plane angle. The system (7), (8) reduces to four coupled equations for θ, ϕ, v_x and v_y [14] with either time periodic boundary conditions for v_x at $z = \pm\frac{1}{2}$ (Couette flow) or time periodic pressure gradient (Poiseuille flow) and appropriate boundary conditions for θ, ϕ. In order to simplify the problem and to gain some understanding of nonlinear director evolution we will treat $v_x(z,t)$ as a prescribed time periodic function with time average $\langle v_x(z,t)\rangle = 0$ and $v_y = 0$. The numerical analysis of the whole set of equations shows that this is a good approximation for small flow amplitudes and moreover, for larger amplitudes this approximation is still reasonable for low frequencies $\omega \ll 1/\tau_v$ ($\delta \ll 1$) [14]. In this approximation $v_x = a(z + 1/2)\cos t$ for Couette flow and $v_x = a(4z^2 - 1)\cos(t)$ for Poiseuille flow where a is the dimensionless flow displacement amplitude. Then the problem reduces to the two coupled nonlinear equations for θ and ϕ which are equivalent to Eq. (7).

For frequencies $\omega \gg 1/\tau_d$ ($\varepsilon \ll 1$), one may introduce a "slow" time $T = \varepsilon t$ for the modulations of the periodic behaviour on the "fast" time scale, so that $\theta = \theta(z,t,T)$, $\phi = \phi(z,t,T)$ and $\partial_t = \partial_t + \varepsilon\partial_T$. Then a systematic perturbation expansion

$$\theta = \theta_0 + \varepsilon\theta_1 + \cdots, \quad \phi = \phi_0 + \varepsilon\phi_1 + \cdots\ , \tag{23}$$

can be formulated where all functions θ_i, ϕ_i are periodic in t. At order ε^0, corresponding to neglect of the elastic coupling (and boundary conditions for the director), one has a continuous two-parameter family of periodic solutions (θ_0, ϕ_0) that can be parametrized by the "phases" $\eta(z,T)$ and $\chi(z,T)$ [12–14]. Thus, θ_0 oscillates around η and ϕ_0 around χ. The solvability conditions for the inhomogeneous linear equations for θ_1 and ϕ_1 at order ε lead to the evolution equations for η and χ that describe the slow evolution of the time-averaged director orientation [13,14]. The time-averaged torques on the director vanish for a simple linear velocity field (Couette flow) whereas for Poiseuille flow (and more general flow fields with $v_{x,zz} \neq 0$) one has torques that tend to orient the director essentially perpendicular to the flow plane. In Fig. 2 the trajectories of the system of evolution equations for η and χ in the absence of other orienting effects (electric and magnetic fields, orienting boundaries) are plotted schematically for a flow-aligning nematic ($\lambda > 0$) and a non-flow-aligning nematic ($\lambda < 0$). For $\lambda > 0$ one has two attractors. However, since for typical nematics θ_{fl} is small, one expects the solution ($\eta = 0$, $\chi = 0$) to be very weakly stable (small

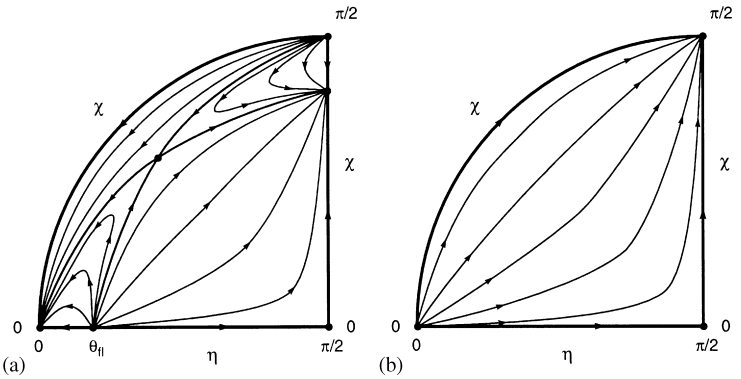

Fig. 2. Phase diagrams for the spatially uniform solutions of evolution equations for $\lambda > 0$ (a) and $\lambda < 0$ (b).

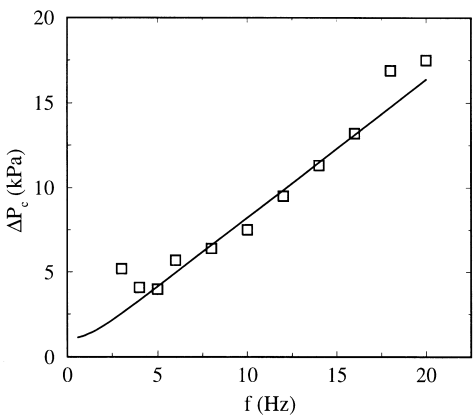

Fig. 3. Frequency dependence of the critical pressure amplitude ΔP_c for out-of-plane transition in MBBA: experimental (squares) and calculated (solid line).

domain of attraction) compared to ($\eta = \pi/2$, $\chi = \chi_0$). For $\lambda < 0$ only the fixed point $\chi = \pi/2$ is stable. In both cases, ($\eta = \pi/2$,$\chi = 0$) is unstable with respect to out-of-plane motion. Clearly, this is different from the case of steady flow with the director initially oriented within the flow plane where even for tumbling motion of the director for non-flow-aligning nematics, the director remains within the flow plane.

Including boundary conditions one obtained the critical flow amplitude for the out-of-plane transition. The threshold found from the linear stability analysis of the evolution equations for η and χ is in a good agreement with the one obtained from the full numerical simulations of Eqs. (7) and (8) [13,14]. This orientational instability in homeotropically oriented nematics under oscillatory Poiseuille flow was recently found experimentally and the frequency dependence of the critical pressure amplitude ΔP_c is plotted in Fig. 3. Using the experimental set-up (Fig. 1b) the transmitted light intensity was measured in the geometry of cross polars with polariser parallel to the flow direction. For amplitudes ΔP below any instability the director oscillates within the flow plane and the intensity is minimal (and constant in time). At some critical pressure amplitude, as a result of an

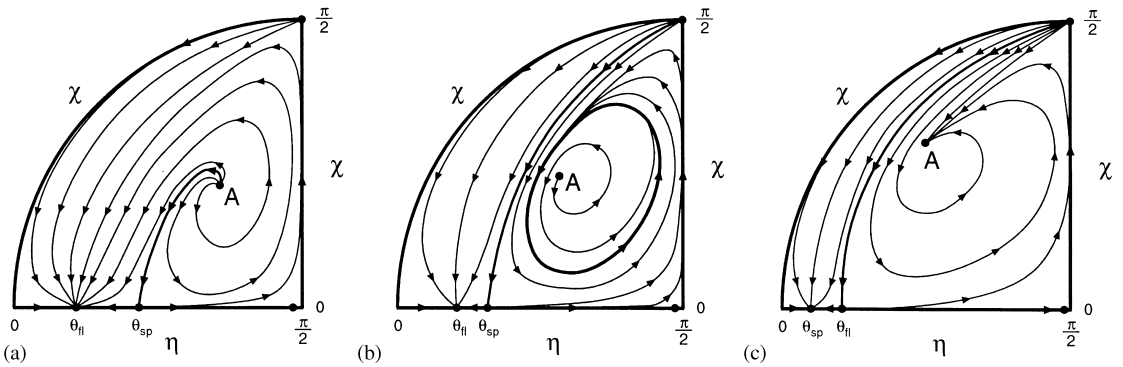

Fig. 4. Plot of trajectories in (η, χ) phase space for the solutions of the evolution equations for $a/h = 1$ (a), $a/h = 2$ (b) and $a/h = 3$ (c). Magnetic field h at the flow-alignment angle θ_{fl}. Note that the director performs rapid oscillations with the external frequency $\omega/2\pi$ around the position (η, χ).

out-of-plane transition, the transmitted light intensity increases and exhibits two rather sharp double peaks over the oscillatory flow period. Since the out-of-plane transition involves the breaking of a two-fold symmetry one expects the appearance of patches of the two states. Indeed, under the microscope we always observed domain boundaries indicating patches of ~ 0.1–1 mm^2 area. After some initial coarsening they did not change much over times of several minutes, except for oscillatory motion of the boundaries with the flow field.

5.3. Slow director oscillations

The analysis of the evolution equations for the time-averaged director motion shows that for oscillatory Poiseuille flow the system can exhibit an interesting bifurcation scenario with a regime of slow limit-cycle oscillations when, in addition, the magnetic field of strength h is applied in the flow plane at the flow-alignment angle θ_{fl}. Such a magnetic field imitates the flow-alignment boundary conditions. The trajectories of the system in (η, χ) phase space are plotted schematically for this case in Fig. 4 for different values of a/h. For values of $a/h < 1.9$ (for MBBA material parameters) [Fig. 4(a)], the orienting effect of the magnetic field is strong compared to the influence of the oscillatory flow, and one has only one attractor ($\eta = \theta_{fl}$, $\chi = 0$), corresponding to the flow-alignment solution ($\theta = \theta_{fl}$, $\phi = 0$) whereas all the other fixed points are unstable. With increasing a/h the flow-alignment solution becomes unstable and a large stable limit cycle appears through a homoclinic bifurcation from the saddle point at $a/h = 1.9$ [Fig. 4(b)]. This limit cycle corresponds to a slow-time periodic out-of-plane motion of the time-averaged (over the oscillatory flow period) director orientation. Further increase of a/h leads to a reduction of the limit cycle and increase of its frequency. It disappears at $a/h = 2.27$ through a supercritical Hopf bifurcation from the spiral point A (we have followed the bifurcation in the reverse sense). For $a/h > 2.27$ point A is stable [Fig. 4(c)] and one has a constant time-averaged out-of-plane director orientation which is characterised (approximately) by η_A, χ_A. In addition θ_{sp} and θ_{fl} cross through each other at $a/h = 2.52$ (for MBBA parameters) thereby exchanging their stability properties.

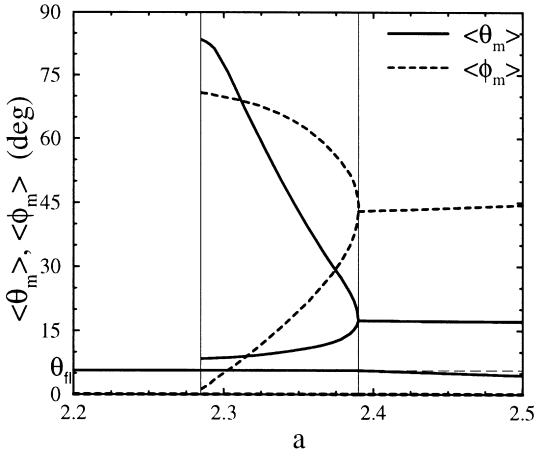

Fig. 5. Bifurcation diagram for $\langle\theta_m\rangle$, $\langle\phi_m\rangle$. Flow alignment boundary conditions; frequency of Poiseuille flow $f = 10$ Hz.

In order to verify the results obtained in the framework of time-averaged approach direct simulations of Eqs. (7) and (8) for oscillatory Couette and Poiseuille flow were performed using central finite differences for the spatial derivatives and the predictor-corrector scheme for the time discretisation. All calculations were made for MBBA material parameters (see Appendix A) and flow frequencies 5 Hz $\leq f \leq$ 100 Hz [14]. We did not find an essential difference between the results obtained using the prescribed velocity field [13] and full numerical simulations with the self-consistent velocity field [14].

We have verified the existence of the stable limit-cycle solutions by simulating Eqs. (7) and (8). The bifurcation diagram as a function of the oscillatory Poiseuille flow amplitude a is shown in Fig. 5. Here the in-plane and out-of-plane director distortions are characterised by the averaged (over the oscillatory flow period) angles $\langle\theta_{\mathrm{m}}\rangle$ and $\langle\phi_{\mathrm{m}}\rangle$ respectively, taken at the midplane of the nematic layer ($z = 0$). We find the limit cycles in a narrow region of the flow amplitudes (the minima and maxima of $\langle\theta_{\mathrm{m}}\rangle$ and $\langle\phi_{\mathrm{m}}\rangle$ are plotted). Clearly, the situation is analogous to that discussed before, where the boundary conditions are replaced by a magnetic field, but the range of existence of the slow-time oscillations here is smaller. The typical temporal evolution of $\langle\theta_{\mathrm{m}}\rangle$ and $\langle\phi_{\mathrm{m}}\rangle$ is shown in Fig. 6. The period of the oscillations is of the order of the director relaxation time τ_{d} (in physical units).

We have also studied a system with planar boundary conditions $[\theta(z = \pm\frac{1}{2}) = 0, \phi(z = \pm\frac{1}{2}) = 0]$ in the presence of an external magnetic field $h = 0.5$ lying in the flow plane at an angle $\theta_{\mathrm{m}} = \pi/4$ with respect to the x-axis. Then, at low amplitudes of oscillatory Poiseuille flow, one has in-plane director oscillations which do not exceed the $\pm\theta_{\mathrm{fl}}$ limit. With increasing flow amplitude a limit cycle corresponding to the slow director oscillations appears as in the previous cases through a homoclinic bifurcation. Further increase of the amplitude a leads to a reduction and disappearance of the limit cycle. The critical flow amplitude a for the limit-cycle instability depends on the value of the magnetic field h and remains very sensitive to the anisotropy of the elastic constants [14].

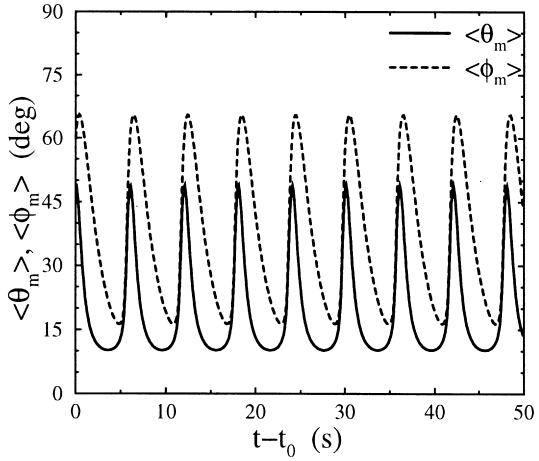

Fig. 6. Slow-time out-of-plane director oscillations. Frequency of Poiseuille flow $f = 10$ Hz; amplitude $a = 2.325$.

6. Roll instability in a homeotropic nematic under Couette flow

We now allow for variations along the shear direction x which leads to a two-dimensional analysis of the nematohydrodynamic equations. Confining $\hat{\boldsymbol{n}}$ and $\boldsymbol{v}$ to the flow plane one can write

$$\hat{\boldsymbol{n}} = \{\cos\theta(x,z,t),\ 0,\ \sin\theta(x,z,t)\}, \quad \boldsymbol{v} = \{v_x(x,z,t),\ 0, v_z(x,z,t)\}\ . \tag{24}$$

The governing equations [7,27,19] are to be supplemented by the boundary conditions. For the velocity one has no-slip boundary conditions

$$v_x(z = -\tfrac{1}{2}) = 0, \quad v_x(z = +\tfrac{1}{2}) = a\cos t\ ,$$
$$v_z(z = \pm\tfrac{1}{2}) = 0 \tag{25}$$

with $a = A_x/d$. For the director we consider the limit of strong homeotropic anchoring

$$\theta(z = \pm\tfrac{1}{2}) = \pi/2\ . \tag{26}$$

For sufficiently small shear amplitudes the director oscillates homogeneously around the homeotropic position (see Section 4), i.e., no x dependence and $v_z = 0$. This basic state loses stability at some critical value a_c of the flow oscillations and then a roll instability sets in with the roll axis perpendicular to the direction of the shear (see Fig. 7). The frequency-dependent critical flow amplitude a_c was measured and calculated numerically from the linear stability analysis of the basic state [19]. We have used for the basic state $(\theta_0,\ v_{0x})$ the solution (15), (16), which is valid for $\delta \ll 1$. Due to the general scaling properties of the problem (see Section 3) one has for the critical flow amplitude a_c and critical wave number of the roll structure q_c:

$$a_c = a_c(\tau_d\omega), \qquad q_c = q_c(\tau_d\omega)\ . \tag{27}$$

The $a_c(\tau_d\omega)$ curve (dotted line) is plotted in Fig. 8 with the experimental data for various thicknesses (40 μm $< d <$ 130 μm). We have also plotted in Fig. 8 the critical amplitude obtained

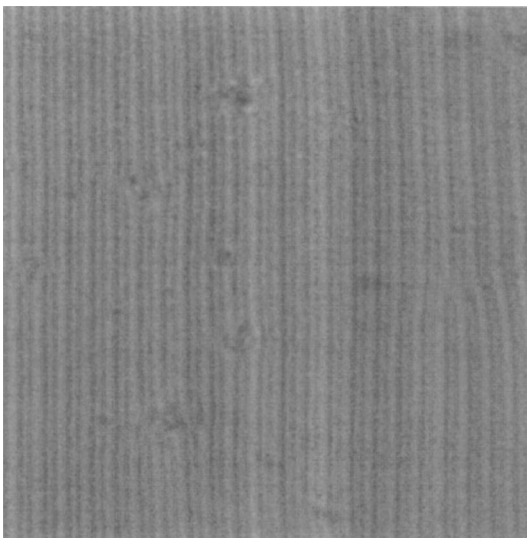

Fig. 7. Roll pattern observed in polarized white light at $f = 80$ Hz and $A_x/d = 0.5$. The rolls are perpendicular to the direction of the upper plate oscillations.

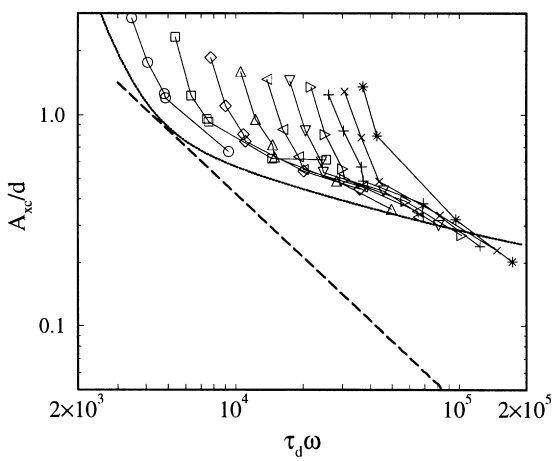

Fig. 8. The normalised threshold amplitude A_{xc}/d for the formation of the roll pattern as a function of the quantity $\tau_d\omega$ for cell thickness $d = 40$ μm (◦), $d = 50$ μm (□), $d = 60$ μm (◇), $d = 70$ μm (△), $d = 80$ μm (◁), $d = 90$ μm (▽), $d = 100$ μm (▷), $d = 110$ μm (+), $d = 120$ μm (×), $d = 130$ μm (∗). The dotted line corresponds to the numerical results of linear stability analysis with fully rigid boundary conditions while the dashed line is calculated from [18].

from the threshold formula of a previous analysis [18] (dashed line). As it is seen our calculations describe the experimental data fairly well except at low frequencies (that correspond to large oscillation amplitudes). The $q_c(\tau_d\omega)$ curve (solid line) is plotted in Fig. 9 together with the experimental data for the thickness $d = 50$ μm.

Our results differ from those reported in Ref. [18] (dashed lines in Figs. 8 and 9) where a small-amplitude approximation for the basic state, the lowest-order time Fourier approximation

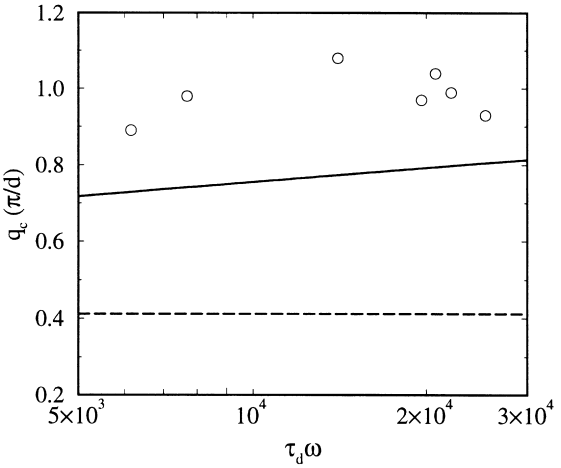

Fig. 9. The wave number (q_c) of the evolving pattern as a function of the quantity $\tau_d\omega$. The continuous line corresponds to the numerical results of linear stability analysis while the dashed line is calculated from [18]. The experimental data (◦) are measured at $d = 50$ μm.

and a one-mode approximation with simple symmetry for the z dependence of the perturbations, as well as some additional simplifications were made. Since the threshold disappears in the formula of Ref. [18] when the inertia term is neglected (it diverges for $\rho \to 0$) the results qualitatively contradict our (essentially rigorous) computations. We found it necessary to go beyond the lowest-order time Fourier approximations and to keep more than one mode with opposite z symmetry. In Fig. 10 we show the "snapshots" of the director and velocity profiles (in x–z plane) for different time moments together with the time-averaged distributions at onset of the roll instability obtained from the numerical linear stability analysis. One can see that there is no $z \to -z$ symmetry as in the director as in the velocity distribution.

7. Slow director precession and nonlinear waves

We have found that a slow precession of the director and associated nonlinear waves can be generated by elliptic shear or oscillatory compression at ultrasonic or at low frequencies. As initial condition the system must be in a continuously degenerated distorted state that can be obtained by homeotropic boundary conditions and an applied external destabilising ($\varepsilon_a < 0$) electric field $\boldsymbol{E} = (0, 0, E_z)$. Alternatively the distorted state can be obtained by having a nematic-isotropic interface inside (and parallel to) the NLC layer produced by a temperature gradient across the sample. Typically the director at such an interface is tilted.

7.1. Elliptic shear

After applying a voltage $U > U_F$ (where U_F is the Fréedericksz threshold) across the layer the director tilts away from the initial homeotropic alignment. The degeneracy with respect to the

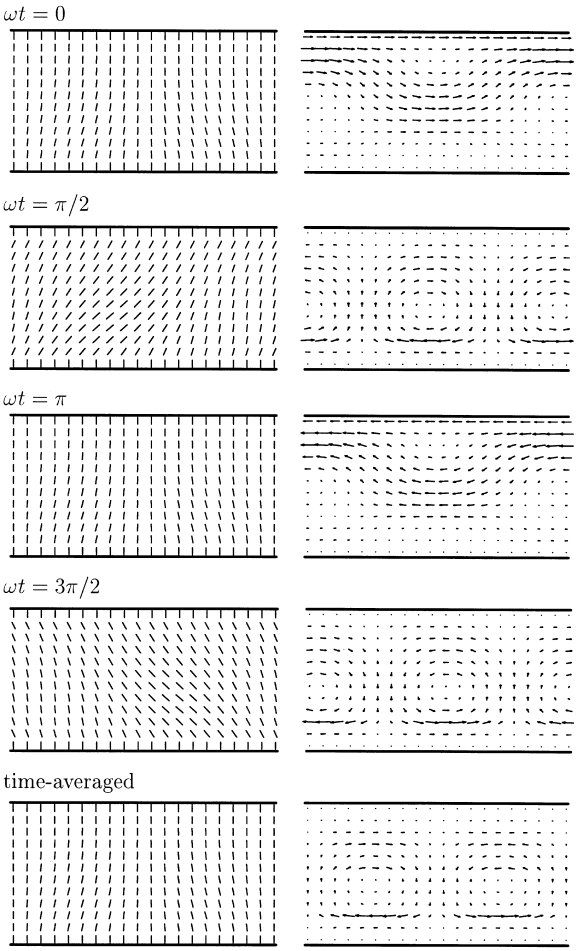

Fig. 10. The director (left) and velocity (right) profiles at onset of the roll instability obtained from numerical linear stability analysis. Shear flow frequency $f = 100$ Hz, critical flow amplitude $a = 0.49$, NLC layer thickness $d = 50$ μm and 5CB material parameters.

azimuthal angle ϕ leads to the well-known "Schlieren texture" observed between crossed polars. After applying the elliptic shear (typically with amplitudes $A/d = 0.2$ and frequency $f = 50$–500 Hz) the director precesses slowly (typical frequency $\Omega \approx 0.1$ Hz) around the z-axis. This precession leads to the movement of dark and bright domains between crossed polars. The precession slows down as the ellipticity is decreased and stops in the case of rectilinear shear.

For frequencies such that $\omega \ll 1/\tau_v$ and small dimensionless shear amplitudes one can use a linear flow field, i.e., complex velocity gradient $V_{,z} = a(\cos t + \mathrm{i}\, b \sin t)$ in Eq. (7) where $a = A_x/d$ and $b = A_y/A_x$ is a measure of ellipticity ($b = 1$ for circular shear). It is useful to neglect first any space dependence, which is a good approximation when the Ericksen number a/ε [6] is large. Consistently, one then also has to discard the electric field, so that in Eq. (7) one is left with the

terms in the first line. Introducing angles by writing $N = \sin\theta \exp i\phi$ one can rewrite Eq. (7) as

$$\theta_{,t} = a'(\cos^2\theta - \lambda\sin^2\theta)[\cos t\cos\phi + b\sin t\sin\phi] ,$$
$$\phi_{,t} = a'\cot\theta[-\cos t\sin\phi + b\sin t\cos\phi] , \tag{28}$$

where $a' = a/(1-\lambda)$. For rectilinear shear ($b = 0$) one recovers the flow-alignment solution $\cot^2\theta = \lambda$, $\phi = 0$.

Eqs. (28) represent a conservative, reversible dynamical system. For $\lambda = 0$ the director is advected passively by the velocity field and Eqs. (28) separate into

$$\partial_t(\tan\theta\cos\phi) = a\cos t , \quad \partial_t(\tan\theta\sin\phi) = ab\sin t . \tag{29}$$

The solutions for arbitrary initial conditions can easily be written. They describe simple, closed 2π-periodic orbits, which either include or exclude the origin ($\theta = 0$, homeotropic orientation). Clearly, this case can be generalised to arbitrary time dependence of the flow.

For circular flow ($b = 1$), Eqs. (28) are integrable even for $\lambda \neq 0$. Then the terms in square brackets become $\cos(\phi - t)$ and $-\sin(\phi - t)$, respectively. Introducing the phase lag $\varphi = \phi - t$ the equations become autonomous. Transforming them into second-order ODE

$$\varphi_{,tt} = (\varphi_{,t} + 1)(2\varphi_{,t} + 1)\cot\varphi - \lambda a'^2\sin\varphi\cos\varphi \tag{30}$$

one can verify that the quantity

$$C = \frac{(\varphi_{,t} + 1 - \lambda a'^2\sin^2\varphi)^2}{(2\varphi_{,t} + 1 - \lambda a'^2\sin^2\varphi)\sin^2\varphi} \tag{31}$$

is a constant of motion. Solving for $\varphi_{,t}$ one obtains the period T of the motion as an integral which can be solved analytically giving

$$T = \int_0^{2\pi} d\varphi/\varphi_{,t} = 2\pi/\sqrt{1 - \lambda a'^2} \tag{32}$$

(independent of C!). For $\lambda \neq 0$ the orbits are in general quasi-periodic. Thus, in addition to the rapid oscillations with ω, the director performs a slow precession with frequency

$$\Omega = \left(1 - \frac{2\pi}{T}\right)\omega \approx \frac{\lambda}{2}\,\frac{A_x A_y}{d^2}\,\omega \tag{33}$$

in physical units. The precession is for flow-aligning materials positive (same sense of rotation as the elliptic shear) and negative otherwise. In Fig. 11 some typical orbits are shown for circular ($b = 1$) and elliptical ($b \neq 1$) shear flow.

The dependence of Ω on the shear amplitude and on the frequency is in accordance with the experimental results [32] (see Fig. 12). However, the system shows a remarkable behaviour when varying the voltage (see Fig. 13). We have illustrated the typical spatio-temporal behaviour of the system with the snapshots taken at different voltages. At sufficiently high voltages the director orientation varies slowly in space and precesses almost homogeneously in time (snapshot 1. in Fig. 13). Around $1.2U_F$ inhomogeneities emit traveling waves and umbilics generate spiral waves (snapshot 2. in Fig. 13), very similar to those observed in oscillatory and excitable chemical reactions [33,34]. The longer waves in the background originate from the lateral cell boundaries.

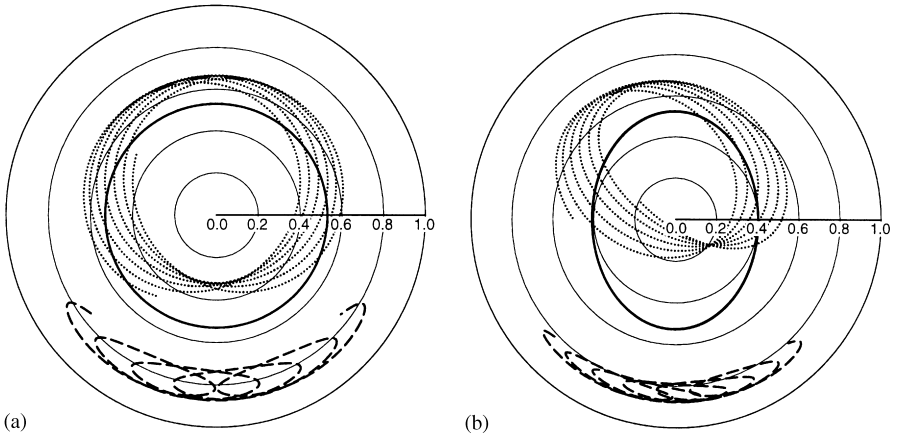

Fig. 11. The orbits of the in-plane director under elliptic shear for $\lambda = 0.2$, $a = 0.5$ and $b = 1$ (a), $b = 0.7$ (b). The thick circle represents a pure rapid rotation around the z axis relevant below the Fréedericksz transition. Other orbits exhibit the slow precession. We show examples with a small average tilt (dotted), expected to be relevant slightly above the FT, and with a large tilt (dashed).

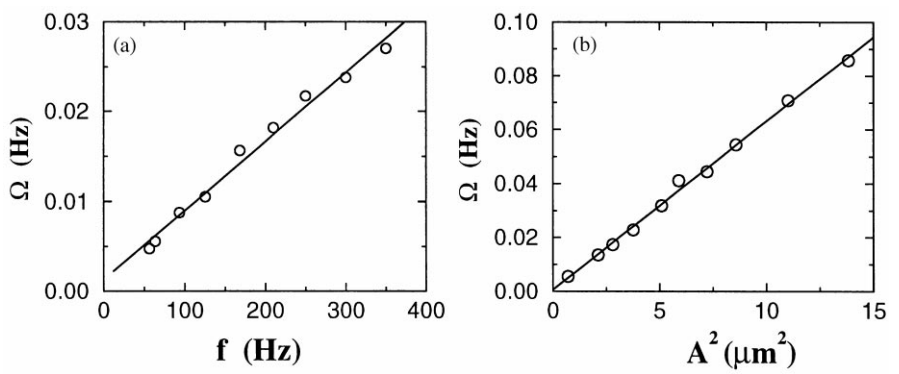

Fig. 12. Precession frequency Ω vs. driving frequency and amplitude. The parameters are: (a) $U/U_F = 2.3$, $d = 20$ μm, $A_x = 0.8$ μm, $A_y = 1$ μm and $T = 25.5°C$. (b) Circular shear, $d = 20$ μm, $f = 122$ Hz, $T = 28.5°C$ and $U/U_F = 2.3$.

At lower voltages spiral pairs seem to be created spontaneously (without umbilics) and one observes spatio-temporal chaos (snapshot 3. in Fig. 13). Although a detailed understanding of this behaviour is still lacking one can understand the qualitative features by noting that in the presence of elliptic shear with b near 1 the Fréedericksz transition transforms into Hopf bifurcation [32].

7.2. Oscillatory compression

A periodic compression of the sample (typical frequencies $f = 1$–100 kHz) also leads to the slow precession of the director [25]. Inhomogeneities in space lead to target-like waves similar to those observed in [35–37] (see Fig. 14, inset). When the phase waves break (in the snapshot) defects

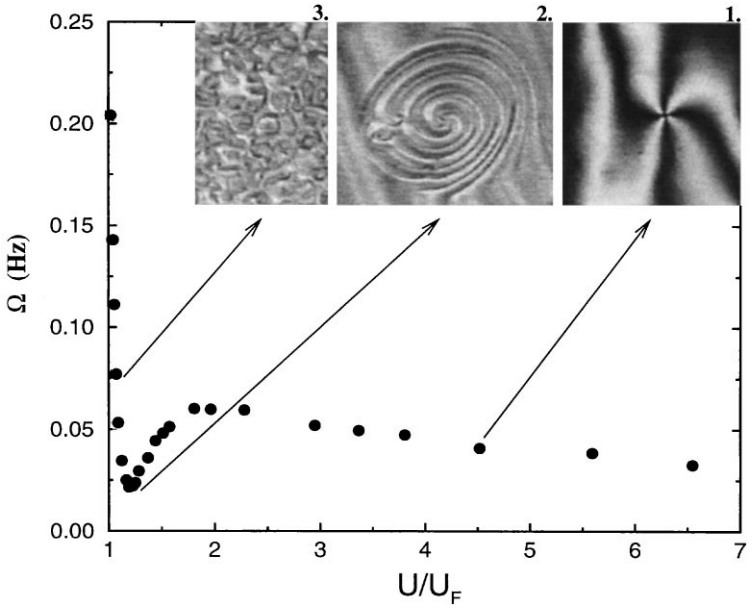

Fig. 13. The frequency of the slow time precession of the director as a function of the applied electric field. The cell thickness $d = 20$ μm, circular shear, $A_x = A_y = 3.4$ μm, $f = 155$ Hz. The spatio-temporal behaviour of the system is considerably different in the three regimes: 1. At large electric fields a nearly homogeneous precession is observed; 2. Around $U = 1.2U_F$ spiral formation has been detected; 3. At smaller voltages ($U < 1.2U_F$) spatio-temporal chaos can be observed.

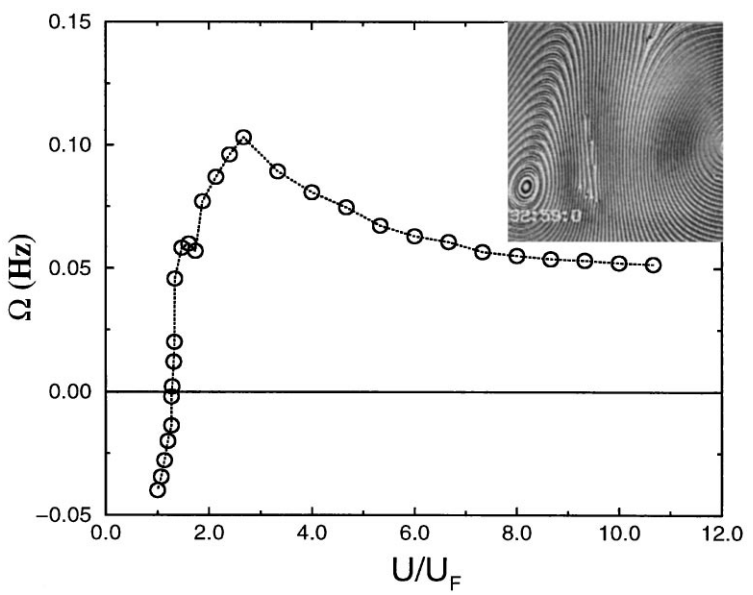

Fig. 14. The frequency of the slow time precession of the director as a function of the applied electric field. The cell thickness $d = 20$ μm, compression amplitude $A_z = 17$ nm and $f = 11.3$ kHz. The snapshot shows a typical "target-like" pattern.

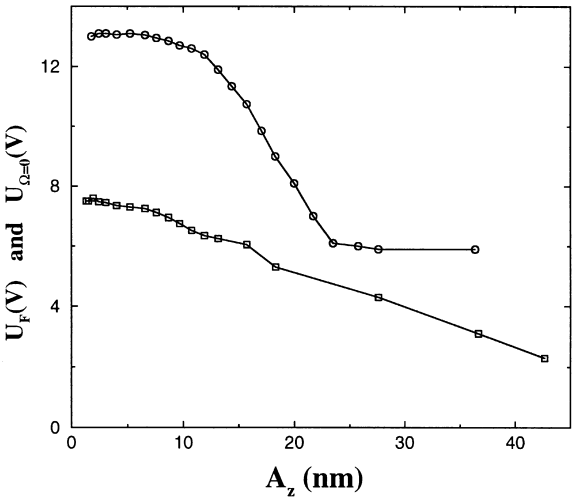

Fig. 15. The critical voltage for Fréedericksz transition U_F (□) and voltage corresponding to the precession reversion $U_{\Omega=0}$ (◯) as a function of the compression amplitude A_z.

appear in the phase wave structure. This effect can be seen in the inset of Fig. 14 in the region where the waves emitted by the two centres collide. As is seen from Fig. 14 at large voltage the slow precession has similar dependence on voltage as in the case of the elliptic shear (Fig. 13). However, approaching U_F from above, the precession stops at $U \approx 1.2U_F$. By further decreasing the voltage the precession reverses ($\Omega < 0$). This interesting result has been observed for MBBA and Phase 5 (MERCK) and was found to be reproducible in several samples. In Fig. 14 the applied voltage is normalised to the voltage corresponding to the Fréedericksz transition in the absence of compression $[U_F(A_z = 0)]$.

We mention that the critical voltage corresponding to the Fréedericksz transition depends on the oscillatory compression. The dependence of the Fréedericksz transition voltage on the compression amplitude A_z (at the location of a target) is plotted in Fig. 15 (squares) together with the voltage corresponding to the precession reversal (circles). Clearly, one can observe the reversal by either changing the voltage or the compression amplitude.

These effects of the precession reversal and decrease of the Fréedericksz transition voltage in the presence of oscillatory compression are not yet understood. From the theoretical point of view the main problem here is the lack of knowledge of the flow field.

8. Conclusion

There is room for further work in all three flow problems considered here. For rectilinear oscillatory Poiseuille flow in a homeotropically oriented sample theory predicts an interesting scenario for boundary anchoring corresponding to the flow-alignment angle or, alternatively, simple planar anchoring of the director with an additional magnetic field in the flow plane at an angle of 45° with respect to the x-axis. Then a transition to a slow time-periodic director precession

has been predicted theoretically (see Section 5.3 [14]). This director motion emerges with increasing flow amplitude through a homoclinic bifurcation and disappears through a Hopf bifurcation. The effect depends strongly on the anisotropy of elastic constants and in fact disappears in the one-constant approximation. It would be interesting to perform experiments to test this prediction.

The mechanism leading to rolls in rectilinear oscillatory Couette flow with its uniform shear rate is quite interesting. We are dealing with a system that is parametrically driven in a time-periodic and, when inertia terms are neglected, essentially spatially *homogeneous* manner (the velocity gradient of the basic flow, which is the relevant quantity, is spatially constant). Then, as long as the state remains homogeneous, the spatial coupling of the director through orientational diffusion is not activated. The system behaves as a zero-dimensional one, which is integrable and cannot develop instabilities. The only way to produce a time-averaged torque on the director is to establish (spontaneously) a space dependence, thereby activating the spatial coupling (and escape integrability). Thus, paradoxically, the diffusive coupling is instrumental in producing the spatial inhomogeneities. The effect is complementary to the mechanism operative in the first case when the driving is *inhomogeneous* (Poiseuille flow) and the director undergoes a *homogeneous* transition. It would be interesting to verify experimentally the structure of the rolls as predicted by theory.

Concerning the director precession under an elliptic shear flow the theory describes the slow precession at large fields essentially quantitatively. The scenario of the waves on the background of the slow precession (diffusive phase waves at large fields changing to amplitude waves with dispersion and eventually Benjamin–Feir chaos at low fields) can be understood qualitatively. There remains to be done a quantitative analysis at low fields as well as an experimental test of the most provocative rediction, namely the reversal of the slow precession for non-flow aligning materials in situations where the elasticity-induced effects are small. Understanding the somewhat similar effects observed under oscillatory compression remains a challenge.

Acknowledgements

We thank O. Tarasov for fruitful discussions and critical reading of the manuscript, S.G. Lipson for providing us piezoelectric drivers and MERCK for providing LC sample materials. A.K. wishes to thank the University of Bayreuth for their hospitality. Financial support from EU Grant TMR-ERBFM-RXCT960085, DFG Grants No. Kr690/12-1, 436RUS113/220, INTAS Grant No. 96-498, MTA Grant No. OTKA-T031808 and VW Grant I/72 920 is gratefully acknowledged.

Appendix A. Material parameters

The numerical computations were carried out for the following MBBA (4-methoxybenzylidene-4′-n-butylaniline) material parameters at 25°C [38,39].

Viscosity coefficients in units of 10^{-3} Ns/m^2:

$$\alpha_1 = -18.1,\ \alpha_2 = -110.4,\ \alpha_3 = -1.1,\quad \alpha_4 = 82.6,\ \alpha_5 = 77.9,\ \alpha_6 = -33.6.$$

Elasticity coefficients in units of 10^{-12} N:

$$K_{11} = 6.66,\ K_{22} = 4.2,\ K_{33} = 8.61,$$

and mass density $\rho = 10^3$ kg/m^3. We used the layer thickness $d = 20$ μm.

For the nematic liquid crystal 5CB (4-n-pentyl-4′-cyanobiphenyl) we took the material parameters at 26°C [40].

Viscosity coefficients in units of 10^{-3} Ns/m^2:

$$\alpha_1 = -6.6,\ \alpha_2 = -77.0,\ \alpha_3 = -4.2,\quad \alpha_4 = 63.4,\ \alpha_5 = 62.4,\ \alpha_6 = -18.4.$$

Elasticity coefficients in units of 10^{-12} N:

$$K_{11} = 5.95,\ K_{22} = 3.77,\ K_{33} = 7.86,$$

and mass density $\rho = 1021.5$ kg/m^3.

References

[1] F.M. Leslie, Arch. Ration. Mech. Anal. 28 (1968) 265.
[2] S.A. Pikin, Zh. Eksp. Teor. Fiz. 65 (1973) 2495 [Sov. Phys. JETP 38 (1974) 1246].
[3] P.E. Cladis, S. Torza, Phys. Rev. Lett. 35 (1975) 1283.
[4] I. Zuniga, F.M. Leslie, Europhys. Lett. 9 (1989) 689.
[5] I. Zuniga, F.M. Leslie, J. Non-Newtonian Fluid Mech. 33 (1989) 123.
[6] E. Dubois-Violette, P. Manneville, in: A. Buka, L. Kramer (Eds.), Pattern Formation in Liquid Crystals, Springer, New York, 1996.
[7] F.M. Leslie, Adv. Liq. Cryst. 4 (1979) 1.
[8] F.M. Leslie, in: J.L. Ericksen, D. Kinderlehrer (Eds.), Theory and applications of Liquid Crystals, Springer, New York, 1987.
[9] J.T. Gleeson, P. Palffy-Muhoray, W. van Saarloos, Phys. Rev. A 44 (1991) 2588.
[10] P. Pieranski, E. Guyon, Solid State Commun. 13 (1973) 435.
[11] P. Pieranski, E. Guyon, Phys. Rev. A 9 (1974) 404.
[12] A.P. Krekhov, L. Kramer, Á. Buka, A.N. Chuvyrov, J. Phys. II 3 (1993) 1387.
[13] A.P. Krekhov, L. Kramer, J. Phys. II 4 (1994) 667.
[14] A.P. Krekhov, L. Kramer, Phys. Rev. E 53 (1996) 4925.
[15] F. Scudieri, Appl. Phys. Lett. 29 (1976) 398.
[16] S.J. Hogan, T. Mullin, P. Woodford, Proc. R. Soc. London, Ser. A 441 (1993) 559.
[17] T. Mullin, T. Peacock, Proc. R. Soc. London Ser. A 455 (2635) 1999.
[18] E.N. Kozhevnikov, Zh. Eksp. Teor. Fiz. 91 (1986) 1346 [Sov. Phys. JETP 64 793].
[19] T. Börzsönyi, Á. Buka, A.P. Krekhov, L. Kramer, Phys. Rev. E 58 (1998) 7419.
[20] P. Pieranski, E. Guyon, Phys. Rev. Lett 39 (1977) 1281.
[21] E. Guazzelli, E. Guyon, J. Phys. France 43 (1982) 985.
[22] E. Dubois-Violette, F. Rothen, J. Phys. France 39 (1978) 1039.
[23] J. Sadik, F. Rothen, W. Besgen, J. Phys. France 42 (1981) 915.
[24] J.-M. Dreyfus, P. Pieranski, J. Phys. France 42 (1981) 459.
[25] T. Börzsönyi, A.P. Krekhov, O.A. Scaldin, Á. Buka, Proceedings of SPIE 3319 (1998) 129.
[26] T. Börzsönyi, Doctoral Dissertation, Budapest, 1998 (in English).
[27] P.G. de Gennes, J. Prost, in: The Physics of Liquid Crystals, Clarendon Press, Oxford, 1993.
[28] M.G. Clark, F.C. Saunders, I.A. Shanks, F.M. Leslie, Mol. Cryst. Liq. Cryst. 70 (1981) 195.
[29] O.S. Tarasov, A.P. Krekhov, Kristallografiya 43 (1998) 516 [Crystallogr. Rep. (Russia) 43 (1998) 476].
[30] W.R. Burghardt, J. Rheol. 35 (1991) 49.

[31] O.S. Tarasov, A.P. Krekhov, Kristallografiya 44 (1999) 1121 [Crystallogr. Rep. (Russia) 44 (1999) 1050].
[32] T. Börzsönyi, Á. Buka, A.P. Krekhov, O.A. Scaldin, L. Kramer, Phys. Rev. Lett. 84 (2000) 1934.
[33] M.C. Cross, P.C. Hohenberg, Rev. Mod. Phys. 65 (1993) 851.
[34] A. de Wit, in: I. Prigogine, S.A. Rice (Eds.), Adv. Chem. Physics, Vol. 109, Wiley, New York, 1999, p. 435.
[35] A.N. Chuvyrov, Zh. Eksp. Teor. Fiz. 82 (1982) 761 [Sov. Phys. JETP 55 (1982) 451].
[36] A.N. Chuvyrov, O.A. Scaldin, V.A. Delev, Mol. Cryst. Liq. Cryst. 215 (1992) 187.
[37] F. Scudieri, Ann. Phys. 3 (1978) 313.
[38] W.H. de Jeu, W.A.P. Claassen, A.M.J. Spruijt, Mol. Cryst. Liq. Cryst. 37 (1976) 269.
[39] H. Kneppe, F. Schneider, N.K. Sharma, J. Chem. Phys. 77 (1982) 3203.
[40] G. Ahlers, in: Á. Buka, L. Kramer (Eds.), Pattern Formation in Liquid Crystals, Springer, New York, 1996.